Probabilistic Engineering Mechanics 26 (2011) 520–527

Contents lists available at SciVerse ScienceDirect

Probabilistic Engineering Mechanics

journal homepage: www.elsevier.com/locate/probengmech

Modeling of seismic wave motion in high-rise buildings

Ray Ruichong Zhang [a,*], Roel Snieder [b], Lotfi Gargab [a], Abdennour Seibi [c]

[a] Division of Engineering, Colorado School of Mines, Golden, CO, United States

[b] Department of Geophysics, Colorado School of Mines, Golden, CO, United States

[c] Department of Mechanical Engineering, Petroleum Institute, P.O. Box 2533, Abu Dhabi, United Arab Emirates

ARTICLE INFO

Article history:
Available online 12 May 2011

Keywords:
Wave-based approach
Seismic responses of buildings
Wave propagation in buildings

ABSTRACT

This study examines one-dimensional wave propagation in a multi-story building with seismic excitation. In particular, the building is modeled as a series of shear beams for columns/walls and lumped masses for floors. Wave response at one location of the building is then derived to an impulsive motion such as displacement and acceleration at another location in time and frequency domains, termed here as wave-based or generalized impulse and frequency response function (GIRF and GFRF), which is dependent upon the building characteristics above the impulse location. Not only does this study illustrate features of GIRF and GFRF in terms of building properties, it also shows broad-based applications of the modeling. Two examples are presented with the use of the modeling. One is wave-based characterization of ten-story Millikan Library in Pasadena, California with the recordings of Yorba Linda earthquake of September 3, 2002. The other is analysis for influence of stochastic floor-to-column mass ratio, story-height and seismic input in seismic wave responses.

1. Introduction

Response analysis and system identification of high-rise buildings with seismic excitation are typically carried out within the framework of vibration theory. In this vibration-based approach, the building structure is modeled as a discrete or a multi-degree-of-freedom (MDOF) system, and structural dynamic properties are characterized with modal frequencies and shapes that are a function of physical parameters such as floor mass and column/wall stiffness. Subsequently, seismic responses are obtainable for a given excitation, and system parameters are identifiable if seismic recordings are provided. Furthermore, structural nonlinear analysis and damage diagnosis are achievable by updating the linear MDOF model to nonlinear one. While this approach is widely used and capable in solving many issues raised in performance-based design and structural vibration control, it has limitation in characterizing comprehensive seismic motion in structures, subsequently affecting the broad-based applications such as effective identification of local system parameters or damage with a limited number of recordings.

The limitation of the vibration-based approach resides in the implicit assumption that seismic responses are *synchronous* at different locations of the structure. In fact, seismic responses are the result of wave propagation in large-scale structures such as high-rise buildings or towers and multiply supported pipelines, in which some wave phenomena such as time delay of traveling waves from one location to the other plays an important role in in-depth understanding of seismic recordings and effective identification of local structural features, as shown in [1–5]. Building upon the aforementioned work as well as pertinent others (e.g., [6–9]), this study proposes one-dimensional seismic wave motion modeling in building structures and examines its effectiveness and broad-based applications. The multi-dimensional wave motion will be examined in the subsequent study.

2. Modeling of wave motion in buildings

In this study, an N-story building is modeled as a series of shear beams for columns/walls and lumped masses for floors as shown in Fig. 1, in which one-dimensional shear wave propagation in vertical direction is investigated.

For source-free, jth column bounded with $(z_{j-1}^{+}, z_{j}^{-}), j = 1, 2, \ldots, N$, wave motion of shear displacement $u(z, t)$ is governed by

$$\frac{\partial^2 u(z,t)}{\partial z^2} = \frac{1}{v_j^2}\frac{\partial^2 u(z,t)}{\partial t^2} \tag{1}$$

where $v_j = \sqrt{G_j/\rho_j}$ is the shear wave speed, and G_j and ρ_j are respectively shear modulus and mass density of the jth column.

* Corresponding author.
E-mail address: rzhang@mines.edu (R.R. Zhang).

0266-8920/$ – see front matter
doi:10.1016/j.probengmech.2011.05.011

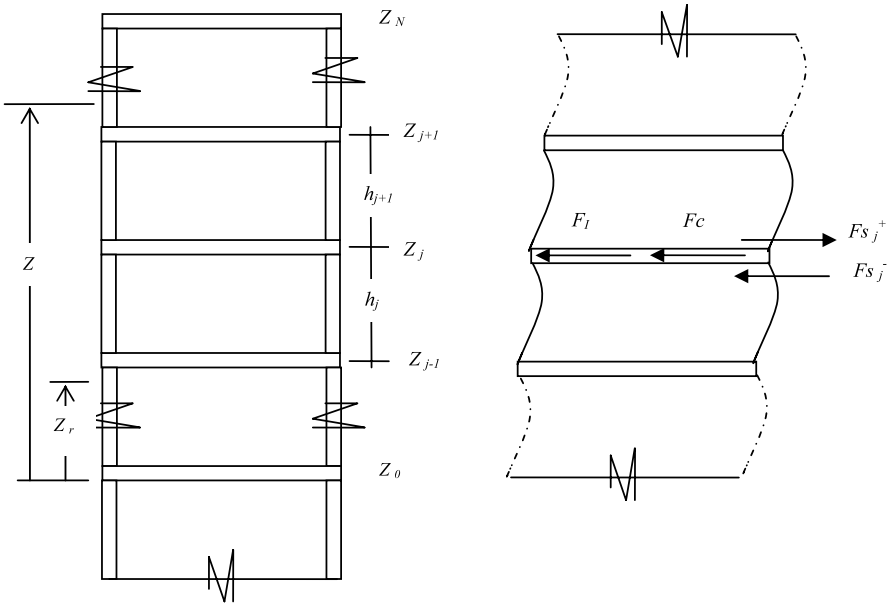

Fig. 1. A model for an N-story building subjected to seismic motion below z_0.

For jth floor bounded with (z_j^-, z_j^+) with $u(z_j^-, t) = u(z_j^+, t)$, the governing equation of wave motion is derived based on Fig. 1 as

$$G_{j+1}A_{j+1}\frac{\partial u(z_j^+, t)}{\partial z} - G_jA_j\frac{\partial u(z_j^-, t)}{\partial z} - c_{fj}\frac{\partial u(z_j, t)}{\partial t} = m_{fj}\frac{\partial^2 u(z_j, t)}{\partial t^2} \tag{2}$$

where the first and second terms ($F_s = GA\partial u/\partial z$) are respectively the shear forces at the positive (superscript $+$) and negative (superscript $-$) sides of the floor height (z_j) due to the shear deformation in the jth and $(j+1)$th columns, the third term ($F_c = c_f\partial u/\partial t$) the floor damping force, and the right-hand side term ($F_I = -m_j\partial^2 u/\partial t^2$) the floor inertia force, in which A is cross-sectional area of the floor/wall, m_f the lumped floor mass which excludes the mass overlapped with columns and walls, and c_f the hysteretic damping coefficient of the floor. For convenience, height z indicates the positive side in this paper and thus superscript $+$ can be dropped in later use.

Introducing Fourier transform representation of the wave motion

$$u(z, t) = \int_{-\infty}^{\infty} U(z, \omega)\mathrm{e}^{\mathrm{i}\omega t}\mathrm{d}\omega, \tag{3a}$$

$$U(z, \omega) = \frac{1}{2\pi}\int_{-\infty}^{\infty} u(z, t)\mathrm{e}^{-\mathrm{i}\omega t}\mathrm{d}t \tag{3b}$$

where i is imaginary unit and ω frequency. Inserting Eq. (3a) into Eqs. (1) and (2), one can solve for wave representation in frequency domain at z and wave-state relationship at z_l and z_m as

$$U_z = U(z, \omega) = U_z^u + U_z^d = C_1\mathrm{e}^{-\mathrm{i}\omega z/v_j} + C_2\mathrm{e}^{\mathrm{i}\omega z/v_j} \tag{4}$$

$$\begin{Bmatrix} U_m^u \\ U_l^d \end{Bmatrix} = \begin{bmatrix} T_{ml} & R_{lm} \\ R_{ml} & T_{lm} \end{bmatrix}\begin{Bmatrix} U_l^u \\ U_m^d \end{Bmatrix} \tag{5}$$

where displacement U_z consists of up-going and down-going waves denoted with superscripts u and d respectively, and transmission and reflection coefficients T_{ml} and R_{lm} (T_{lm} and R_{ml}) relate the out-going waves U_m^u and U_l^d to input waves U_l^u and U_m^d for building segment bounded with (z_l, z_m), as seen in Fig. 2.

For the jth column, coefficients T and R can be found as

$$T_{j^-(j-1)} = T_{z_j^- z_{j-1}} = \mathrm{e}^{-\mathrm{i}\omega h_j/v_j} = T_{(j-1)j^-},$$
$$R_{j^-(j-1)} = R_{(j-1)j^-} = 0. \tag{6}$$

To understand the transmission coefficient in time domain, one can perform inverse Fourier transform with Eq. (3b) for Eq. (6) and obtain transmission coefficient in time domain as

$$\tilde{T}_{j^-(j-1)}(t) = \frac{1}{2\pi}\int_{-\infty}^{\infty}\mathrm{e}^{-\mathrm{i}\omega h_j/v_j}\mathrm{e}^{\mathrm{i}\omega t}\mathrm{d}\omega = \delta(t - h_j/v_j) \tag{7}$$

which shows the delta function δ with time delay h_j/v_j, meaning the up-going impulsive wave propagation through column height without loss of amplitude. Wave attenuation in propagation due to damping can be taken into consideration by replacing real shear wave speed with complex one $v_j[1 + \mathrm{i}\gamma_{cj}|\omega|]$ with γ_c indicating the hysteretic damping ratio (e.g., [8]), which is equivalent to multiplying a frequency-dependent attenuation factor $B_j = \mathrm{e}^{-\gamma_{cj}|\omega|h_j/v_j}$ in Eq. (6) (e.g., [3]).

For the jth floor, one can find

$$T_{jj^-} = \frac{2}{1 + r_{l_j} - r_{D_j} + \mathrm{i}r_{M_j}} = B_{fj}\mathrm{e}^{-\mathrm{i}\omega h_{ej}/v_j}$$
$$R_{jj^-} = T_{jj^-} - 1, \qquad T_{j^-j} = T_{jj^-}r_{l_j}, \qquad R_{j^-j} = T_{j^-j} - 1 \tag{8}$$

where coefficients r_{lj}, r_{Dj} and r_{Mj}, amplitude B_{fj} and equivalent floor height h_{ej} can be found in terms of column impedance (ρv) ratio, cross-sectional area (A) ratio, floor-to-column mass ratio (r_m), wave traveling time for column length (h/v), i.e.,

$$r_{l_j} = \frac{\rho_{j+1}v_{j+1}}{\rho_j v_j}\frac{A_{j+1}}{A_j}, \qquad r_{D_j} = \gamma_{fj}r_{M_j},$$
$$r_{M_j} = r_{m_j}\frac{h_j}{v_j}\omega, \qquad r_{m_j} = \frac{m_{f_j}}{m_j}$$
$$B_{f_j} = \frac{2}{\sqrt{(1 + r_{l_j} - r_{D_j})^2 + r_{M_j}^2}},$$
$$h_{ej} = \frac{v_j}{\omega}\tan^{-1}\frac{r_{M_j}}{1 + r_{l_j} - r_{D_j}}. \tag{9}$$

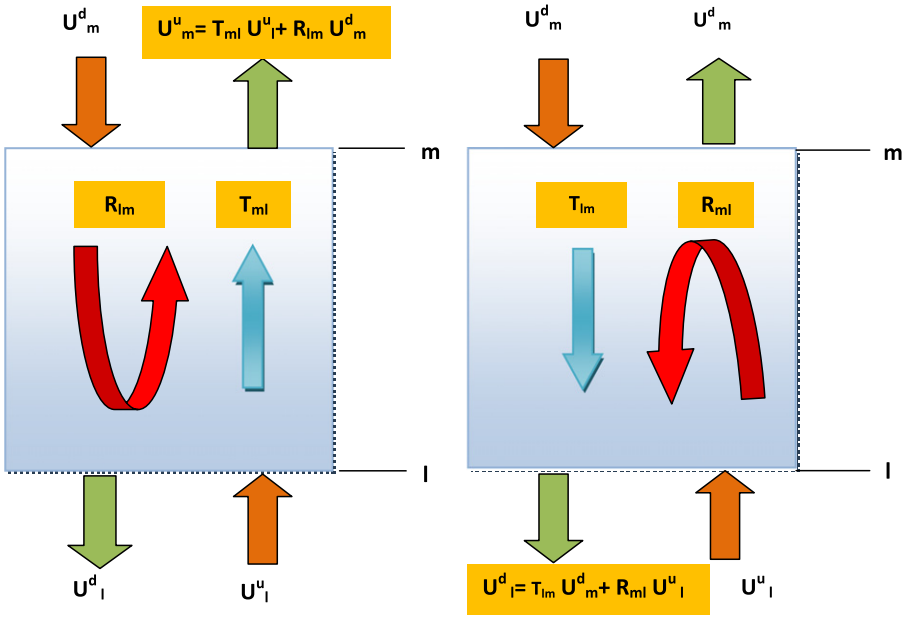

Fig. 2. Transmission and refection coefficients T_{ml} and R_{lm} ((a) left) or T_{lm} and R_{ml} ((b) right) relate the out-going wave U_m^u (left) or U_l^d (right) and input waves U_m^d and U_l^u in building segment bounded by (z_l, z_m) or (l, m).

With Eqs. (6)–(7) as a reference, Eqs. (8)–(9) indicate that lumped floor mass can be treated as a column-type continuum with equivalent height and damping but with non-zero reflection coefficients.

For lumped mass at the free building top, $\rho_{N+1} = v_{N+1} = A_{N+1} = 0$ or $r_{I_N} = 0$, which degenerates Eq. (8) to $T_{NN^-} = 2$ and $R_{NN^-} = 1$, meaning that up-going wave $U_{N^-}^u$ is transmitted to the top with doubled amplitude and also reflected to down-going wave $U_{N^-}^d$ without changing the motion direction.

At the building lower end z_0 (or generally at referenced location z_r which could be selected as z_0), no segments below level z_0 are used in the model, yielding $r_{I_1} = \infty$. One can then find $T_{0^-0} = 0$ and $R_{0^-0} = -1$, suggesting down-going wave U_0^d is completely reflected to the up-going wave U_0^u with changing the motion direction. While this feature will not be used in subsequent response calculation, it can help interpret wave phenomena at lower end z_0 with a fixed boundary.

For a composite building segment bounded with (z_l, z_n), or simply (l, n), with intermediate location z_m $(z_l < z_m < z_n)$ such as (z_{j-1}, z_j) with z_j^-, repeat use of Eq. (5) for (l, m) and (m, n) will lead to the representation of transmission and reflection coefficients in (l, n) in terms of those in two sub-segments in (l, m) and (m, n) as

$$T_{ln} = \frac{T_{lm}T_{mn}}{1 - R_{nm}R_{lm}}, \qquad R_{ln} = R_{mn} + \frac{T_{nm}R_{lm}T_{mn}}{1 - R_{nm}R_{lm}}. \tag{10}$$

The above composition rule can be applied reversely for (n, l) and also repeatedly to find all the transmission and reflection coefficients between any two locations.

With the aforementioned coefficients R and T, wave response at z (or $z_R = z - z_r$) can then be related to those at referenced level z_r that could be at the bottom of the building or any other height as

$$D_{Rr}(\omega) = \frac{U_{z_R}}{U_{z_r}} = \frac{(1 + R_{NR})T_{Rr}}{(1 - R_{rR}R_{NR})(1 + R_{Nr})}, \tag{11a}$$

$$d_{Rr}(t) = \int_{-\infty}^{\infty} D_{Rr} e^{i\omega t} d\omega. \tag{11b}$$

Eq. (11a) indicates that D_{Rr} is dependent only upon R and T above z_r which are function of building properties in frequency domain. For $z = z_r$, Eqs. (11a), (11b) lead to $D_{Rr} = 1$ and $d_{Rr} = \delta(t)$, suggesting that D_{Rr} and d_{Rr} are respectively frequency and time displacement responses at z (z_R) to displacement impulse at z_r. Subsequently, wave response representation in general, and displacement response at z to input displacement at z_r in particular, is then found as

$$u(z, t) = \int_{-\infty}^{\infty} D_{Rr} U_{z_r} e^{i\omega t} d\omega = \int_{-\infty}^{\infty} d_{Rr}(t - \tau) u(z_r, \tau) d\tau \tag{12}$$

which has the same mathematical form as traditional vibration response representation in frequency domain with D_{Rr} as frequency response function and in time domain (Duhamel's or convolution integral) with d_{Rr} as impulse response function.

While the aforementioned derivation is for displacement (u, U), it is straightforward to extending to velocity $(v = du/dt, V = i\omega U)$ and acceleration $(a = d^2u/dt^2, A = -\omega^2 U)$ with D_{Rr} and d_{Rr} remaining the same. For acceleration input at z_r and displacement response at z, which is the typical case for displacement response to earthquake ground acceleration, Eq. (12) can be modified as

$$u(z, t) = \int_{-\infty}^{\infty} H_{Rr} A_{z_r} e^{i\omega t} d\omega = \int_{-\infty}^{\infty} h_{Rr}(t - \tau) a(z_r, \tau) d\tau \tag{13}$$

where $H_{Rr} = -D_{Rr}/\omega^2$ and h_{Rr} have conventional meanings for frequency response function and impulse response function respectively. Because of the aforementioned difference, D_{Rr} and d_{Rr} are referred to respectively as wave-based or generalized frequency response function (GFRF) and generalized impulse response function (GIRF).

3. Applications in earthquake engineering

For illustration, two examples are presented below to show the usefulness and effectiveness of the proposed modeling in system identification and seismic response analyses.

3.1. Wave phenomena and vibration features with uniform shear-beam model

To show the wave-based modeling and characterization of seismic responses and system identification other than vibration-

based one, one can first examine a special case for the aforementioned model, i.e., uniform shear–beam model without lumped floor mass, which leads Eq. (11a) to

$$D_{Rr} = \frac{[1 + e^{-i\omega(2H_r - 2z_R)/v_c} e^{-\gamma_c|\omega|(2H_r - 2z_R)/v_c}]e^{-i\omega z_R/v_c} e^{-\gamma_c|\omega|z_R/v_c}}{1 + e^{-i\omega(2H_r)/v_c} e^{-\gamma_c|\omega|(2H_r)/v_c}} \tag{14}$$

where $H_r = z_N - z_r$ and v_c denotes respectively the height and shear wave velocity of the building portion bounded by (z_r, z_N). The GIRF can be found by substituting GFRF of Eq. (14) into Eq. (11b), where the integration can be evaluated with the method of residues. In particular, the integrand for d_{Rr}, a function of the real variable ω, is treated as a function of variable y, which has an infinite number of poles y_j $(j = 1, 2, \ldots)$ in the upper half complex plane, namely

$$\begin{aligned} &1 + e^{-iy(2H_r)/v_c} e^{-\gamma_c|y|(2H_r)/v_c} = 0 \\ &y_j = (\pm 1 + i\gamma_c)\omega_j, \qquad \omega_j = (2j-1)\omega_0, \\ &\omega_0 = \frac{\pi v_c}{2H_r}, \quad j = 1, 2, \ldots, \infty. \end{aligned} \tag{15}$$

The integration of Eq. (11b) can be found as

$$d_{Rr} = 8\omega_0 \sum_{j=1}^{\infty} (-1)^{j+1} e^{-\gamma_c \omega_j t} \cos\frac{\omega_j(H_r - z_R)}{v_c} \sin(\omega_j t). \tag{16}$$

Eq. (16) shows GIRF consists of infinite number of motion modes, each of which has exponentially decaying damping factor, modal shape with cosine factor, and sinusoidal motion with modal frequency ω_j. The fundamental or first mode with $j = 1$ has period $T_c = 4H_r/v_c$ which is the travel time for waves to propagate up and down the building height (H_r) twice. Eqs. (14)–(16) are first derived in [3].

To validate usefulness of the aforementioned uniform shear–beam model, this study follows [3] to examine seismic recordings in ten-story Millikan Library shown in Fig. 3 after the Yorba Linda earthquake of September 3, 2002. Fig. 4 shows the seismic acceleration recordings in the north–south component in the west side of the building at basement and the 1st to 10th floor. While features of wave propagation in the building can be observed from the arrival time of traveling waves from floor to floor in 10–11 s, it can be seen clearly through GIRF extracted from the recordings.

To extract GIRF from recordings, one can first calculate the recording-based GFRF, i.e.,

$$\tilde{D}_{jb} = \frac{\tilde{U}_j \tilde{U}_b^*}{|\tilde{U}_b|^2 + \varepsilon} \underset{\varepsilon \to 0}{\Rightarrow} \frac{\tilde{U}_j}{\tilde{U}_b} \tag{17}$$

where $\tilde{U}$ is the recording in frequency domain, superscript asterisk indicates the complex conjugate, and ε is a positive small number, implying the added white noise. The white noise is used primarily to avoid unstable calculation of GFRF at some frequencies near the notches in the spectrum $\left|\tilde{U}_b\right|^2$, as suggested in [3]. As ε approaches zero, $\tilde{D}_{jb}(\omega) \Rightarrow \frac{\tilde{U}_j}{\tilde{U}_b}$, the definition of GRFR. With the use of Eq. (11b), the GIRF of the building at different floors ($j = 1$–10) with respect to referenced motion at basement (b), denoted as $\tilde{d}_{jb}$, are then found, which is shown in Fig. 5 with ε selected as 5% of total power spectrum of basement motion. Note that the tilde over quantities d, D and U is used to distinguish the recording-based quantities from those based on modeling or Eqs. (14) and (16).

As shown in Fig. 5, the GIRF at the basement is impulsive acceleration. As a fictitious input or virtual source to the building, the impulsive acceleration at basement or the peak for visual convenience at $t = 0$ is propagated upward at building shear velocity, and time delay of the peak at increasing height is well

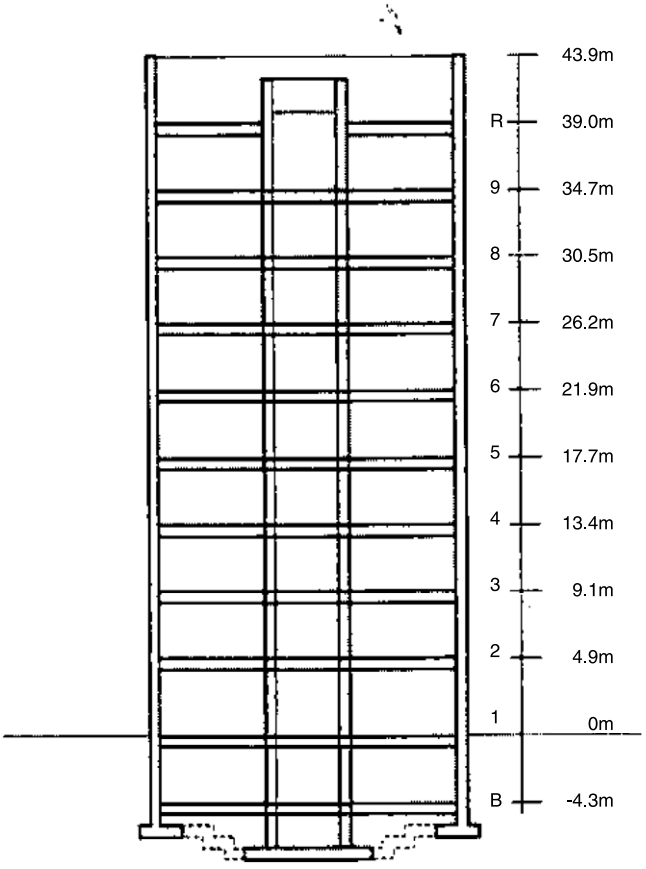

Fig. 3. Vertical cross section of the Millikan Library in the north–south direction.

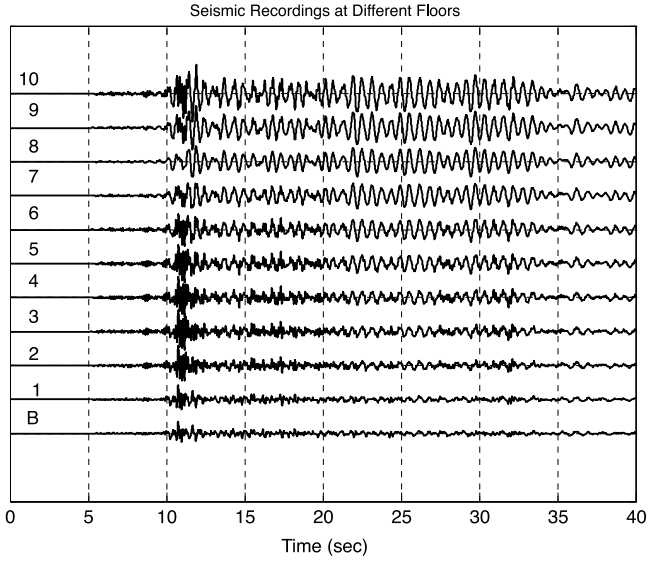

Fig. 4. Seismic recordings at the different floors (indicated as 1–10) with respect to basement motion (indicated as B or b).

observed. After hitting the top, the peak is reflected completely without changing motion direction due to the reflection feature at free top ($R_{NN} = 1$). The time delay of the waves traveling upward from the 10th floor to the top and then downward to the 10th floor generates the second peak at the 10th floor. The 2nd peak is then propagated downward and disappear at the basement due to the fact that the basement with impulsive acceleration is equivalent to the fixed basement end, which makes the wave motion disappear at time other than $t = 0$. This phenomenon can

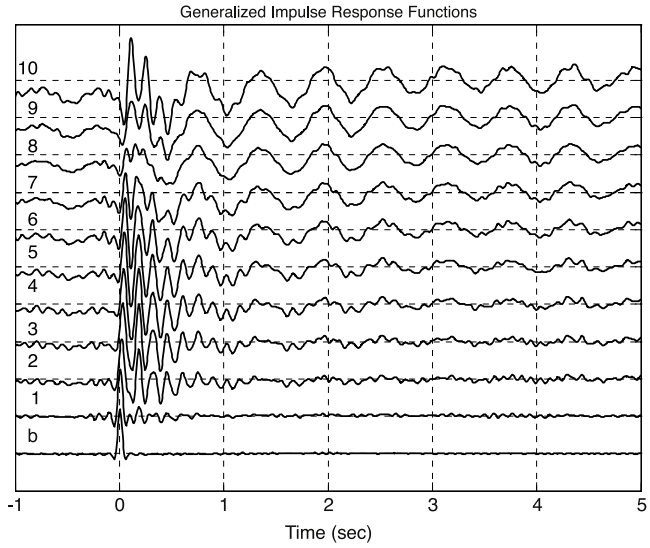

Fig. 5. GIRFs at the different floors (indicated as 1–10) with respect to basement motion (indicated as B or b).

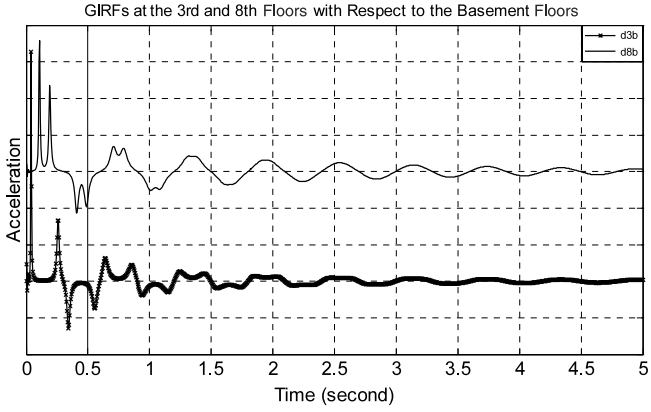

Fig. 6. GIRFs at the 3rd and 8th floors with respect to basement motion obtained based on Eq. (14) with selected parameters $v_c = 322$ m/s, $H_r = 48.2$ m, $\gamma_c = 0.044$.

also be explained with transmission and reflection coefficients at the basement ($T^-_{bb} = 0$ and $R^-_{bb} = -1$), which indicates that all the down-going waves completely to the up going waves reflected at the basement, i.e., fixed basement boundary. When the 2nd peak reaches the basement, another up-going impulsive wave will be generated with the same amplitude but opposite motion direction, making the fixed basement motionless at that time instant.

The aforementioned cycle of wave propagation continues as time goes on. For earlier time (0–1 s), the GIRF consists primarily of superposition of up-going and down-going traveling shear waves. For later time (>1 s) as the traveling waves can be regarded as standing waves, the GIRF develops the building dynamic features characterized by modal frequencies (primarily by the 1st mode or the building resonance), with the amplitude reduced as time goes on (e.g., see GIRF at the 10th floor), which is typically the free vibration or impulse response phenomenon. The increased amplitude of the GIRF at the fundamental modal frequency with the position changed from the 1st to the 10th floor is again attributed to the wave phenomena due to the fixed bottom and free top boundaries.

All the aforementioned wave features extracted from recordings can be observed more clearly with the use of Eq. (16), as shown in Fig. 6 for the modeling-based GIRFs at the 3rd and 8th floor with respect to basement motion, in which building shear wave velocity

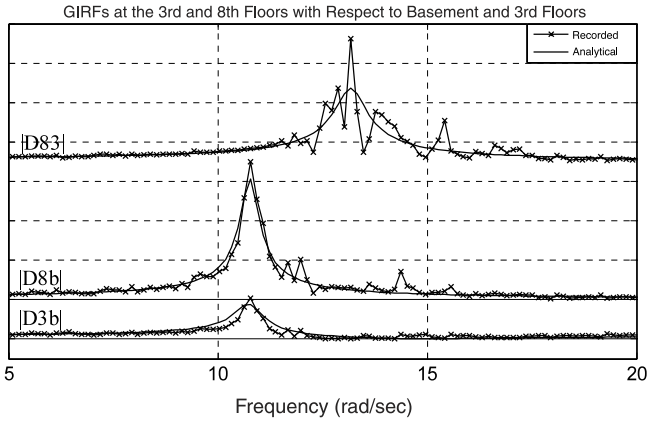

Fig. 7. Magnitudes of GFRF at the 3rd and 8th floors with respect to basement and 3rd floor motion obtained based on seismic recordings and theory in Eq. (14).

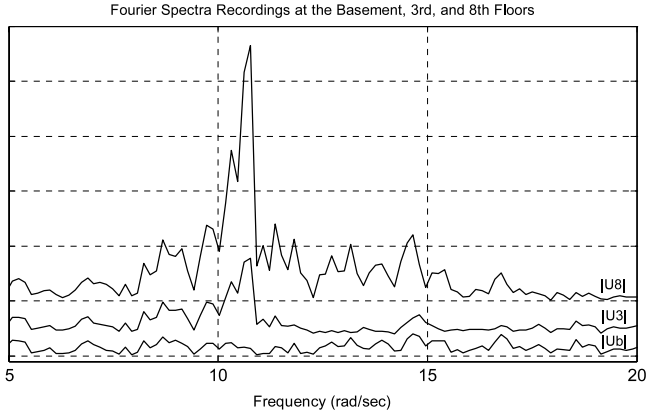

Fig. 8. Fourier spectra of seismic recordings at the basement, 3rd and 8th floors.

322 m/s and damping factor 0.0244 are used based on the study in [3]. In particular, the first peak at the 3rd floor is rooted from the impulse propagation from the basement, which propagates to the first peak at 8th floor with damping-related reduced amplitude. That first peak at the 8th floor is then propagated to the top and then reflected to travel downward to the 8th and 3rd floors to generate the second peaks with sequential reduced amplitude. The second peak at the 3rd floor continues propagating downward to the basement. Since the motion will disappear at basement due to the fixed boundary, a negative, same amplitude peak, balancing the positive one at the basement, is generated and propagated upward. That negative peak propagates to the 3rd and 8th floors with further reduced amplitude, and continues following previous wave propagation cycle. From perspective of vibration at the 8th floor (similar to the other locations), the first couple of peaks are the result of initial condition, for the impulse response in a system is equivalent to the free vibration with non-zero initial condition. As time goes on, the vibration feature at that floor is then dominated by the character of the resonance of whole building, while high-order motion modes are also involved.

In addition, the model can help identify some building features, exemplified as shear wave speed and damping with the use of two sets of recordings. Fig. 7 shows the GFRFs of acceleration at the 3rd and 8th floors with respect to referenced motion at basement and the 3rd floor respectively based on recordings (i.e., $\tilde{D}_{8b}$, $\tilde{D}_{3b}$ and $\tilde{D}_{83}$) and the uniform shear–beam model (i.e., D_{8b}, D_{3b} and D_{83}). For reference, the Fourier spectra of the seismic recordings at the three locations are also shown in Fig. 8. The identified shear wave speeds for the whole building and the 3rd-floor-up building portion are

Table 1
Identified shear wave speeds and damping and their comparison with results from others (one number from Snieder and Safak [3] using the uniform shear–beam model and the same earthquake but averaged over all D_{jb} , $j = 1$–10 with 11-set recordings) and (two numbers from Table 11.1.1 in [10] with Lytle and San Fan Fernando earthquake recordings respectively).

	Height (H_r) and location (z_R) in m	Identified 1st modal frequency in rad/s	Shear wave speed in m/s	Damping
$z_r = z_b$ $z = z_3$	48.2, 13.4	10.77 (12.08,10.13)	330 (322)	0.0305 (0.0244) (0.029,0.064)
$z_r = z_b$ $z = z_8$	48.2, 34.8	10.77 (12.08,10.13)	330 (322)	0.0281 (0.0244) (0.029,0.064)
$z_r = z_3$ $z = z_8$	34.1, 21.4	13.16	292	0.0187

330 and 292 m/s respectively, indicating that shear modulus (G) of the 3rd-floor-up building portion is less than that of the whole building if mass density (ρ) is assumed the same. Alternatively, the lower portion of the building (i.e., from the basement to the 3rd floor) is more rigid in shear resistance than the upper portion (from the 3rd floor to the top). Typically, the stronger the shear rigidity of the building is, the less the corresponding damping ratio. While not universally correct, this phenomenon is also observed from the identified damping for the aforementioned case, i.e., 0.0281 and 0.0187 respectively for the whole and the 3rd-floor-up building portion. As shown in Table 1, the identified parameters are also compared with those using recordings at other floors as well as those from [10,3], indicating that the uniform shear–beam model is good enough to characterize the fundamentals of wave and vibration motion in buildings.

3.2. Deterministic and stochastic features of wave motion with general floor–beam model

The difference between earthquake recordings and uniform shear–beam model is well observed exemplified in Fig. 7, which is primarily attributed to the deterministic modeling and analysis without considering other major building features such as floor masses. This issue can however be addressed with a stochastic wave motion model with floor masses, in which building parameters and/or seismic input are treated as random variables/processes. While various statistical responses for the stochastic model can be found within the framework of probabilistic structural dynamics (e.g., [11]), this study presents some analyses with selected system parameters in wave responses and stochastic seismic acceleration input at building bottom.

For regular buildings, column/wall properties are not changed significantly from one floor to the other, and can be assumed the same without loss of generality. For earthquake-excited building motion, the largest frequency of interest is typically less than $n\omega_1$ with $n < N$. Therefore, for random floor mass with small floor-to-mass ratio ($r_{mj} = m_{fj}/m_{cj} \ll 1$), Eqs. (8)–(9) become

$$T_{jj^-} = T_{j^-j} \approx \mathrm{e}^{-\mathrm{i}\omega h_{ej}/v_j}, \qquad h_{ej} \approx 0.5 r_{m_j} h_j \tag{18}$$

which suggests that up-going and down-going waves transmit through the jth floor without loss of amplitude. As far as transmission coefficients are concerned, the floor functions like an extended column portion with extra height h_{ej} and zero damping. Accordingly, transmission coefficients for a building segment with a column connected to a floor mass are equivalent to those in a pure column without floor, but with an increased column length ($h_j + h_{ej}$) and reduced damping factor ($\gamma_{ej} = \gamma_{cj}/(1 + h_{ej}/h_j)$). Alternatively, they can also be viewed as the equivalent transmission coefficients in the same column length but with decreased velocity and reduced damping factor. Based on Eq. (15), the fundamental modal frequency of the building with floor masses, denoted as Ω_1, is decreased in comparison with that without floor masses (ω_1). This can be seen clearly

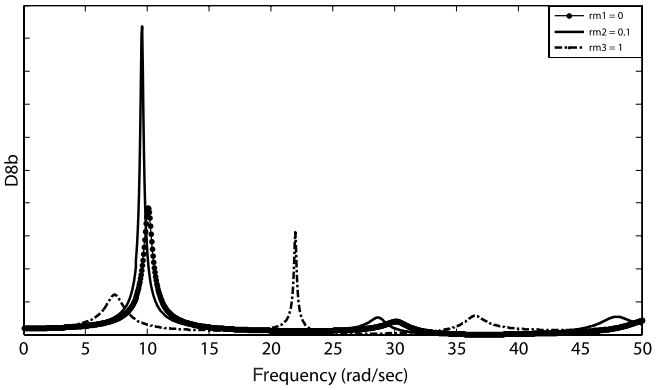

Fig. 9. GFRFs (D_{8b}) at the 8th floor of a 11-story building with respect to bottom motion with $v_j = 300$ m/s, $h_j = 4.25$ m, $\gamma_{cj} = \gamma_{fj} = 0.03$, $r_{1j} = 1$ and $r_{m11} = 0.5 r_{m10}$, for $j = 1, 2, \ldots, 11$.

in Fig. 9 with $r_{mj} = 0$ and 0.1, where $r_{mj} = 0$ is associated with the uniform shear–beam model. The corresponding response amplitude is increased due to the reduced damping. For high-order mode motion ($j > 1$), the modal frequencies Ω_j of the building with floor masses will be reduced proportionally and the corresponding amplitude will be increased in general. The mean μ and standard variation σ of modal frequency Ω_j can be found as

$$\mu_{\Omega_j} = \omega_j\{1 - 0.5\mu_{r_m}\}, \qquad \sigma^2_{\Omega_j} = 0.25\mu^2_{\Omega_j}\sigma^2_{r_m} \tag{19}$$

where μ_{rm} and σ_{rm} are the mean and standard deviation of random floor-to-column mass ratio. It can be proved that if r_{mj} ($j = 1, 2, \ldots, N$) is constant and floor height h_j is random, Eq. (19) remains the same except μ_{rm} and σ_{rm} replaced by μ_h and σ_h respectively. The other statistical responses such as mean and standard deviation of frequency response amplitudes at corresponding modal frequencies can be found numerically based on Eqs. (14), (16) and (19).

For large floor-to-column mass ratio or other random system parameters, the statistical analysis for GIRF/GFRF must be carried out numerically or with Monte Carlo simulation. While not presented here, this paper shows influences of some system parameters in frequency responses. In particular, Fig. 9 shows the influences of large floor-to-column mass ratio ($r_{mj} = 1$) in GFRF, revealing similar phenomena observed with small r_{mj} before. Fig. 10 indicates that modal frequencies are insensitive to the change of column impedance ratio r_I, while the corresponding amplitudes are reduced significantly with decreased r_I.

For ground motion characterized by stationary stochastic process [11]

$$a(z_0, t) = \int_{-\infty}^{\infty} \mathrm{e}^{\mathrm{i}\omega t}\mathrm{d}Z(\omega) \tag{20}$$

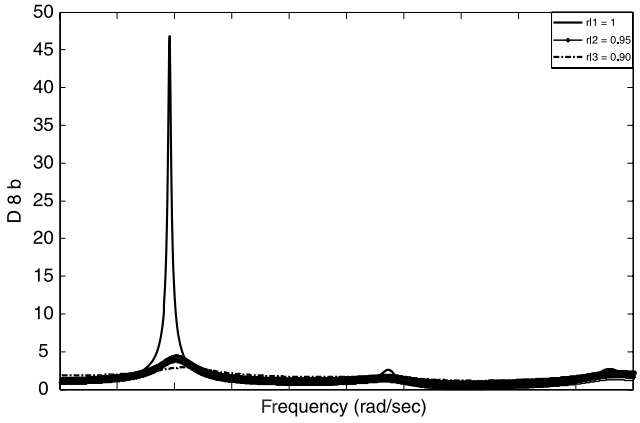

Fig. 10. GFRFs (D_{8b}) at the 8th floor of a 11-story building with respect to bottom motion with $v_j = 300$ m/s, $h_j = 4.25$ m, $\gamma_{cj} = \gamma_{fj} = 0.03$, $r_{mj} = 0.1$ and $r_{m11} = 0.5r_{m10}$, for $j = 1, 2, \ldots, 11$.

where Z is a stochastic process with orthogonal increment in frequency, the mean square acceleration response with deterministic building parameters can be found as

$$E[a^2(z,t)] = \int_{-\infty}^{\infty} \Phi(\omega)\mathrm{d}\omega, \quad \Phi(\omega) = D_{R0}^2(\omega)G(\omega) \tag{21}$$

where E denotes ensemble average, and G and Φ are spectral densities of ground acceleration and response respectively. For Kanai–Tajimi spectrum selected for the stochastic ground motion characterization, i.e., $G = G_0(1 + 4\xi^2\omega^2/\omega_g^2)/[(1 - \omega^2/\omega_g^2)^2 + 4\xi^2\omega^2/\omega_g^2]$, Fig. 11(a) shows the spectral densities of acceleration at the 8th floor with seismic input at alluvium and rock sites. Since the rock predominant frequency ($\omega_g = 27$ rad/s) is closer to the second modal frequency ($\omega_2 \sim 22$ rad/s) than the alluvium one (18.4 rad/s), the peak with rock at the second modal frequency is larger than that with alluvium. This can also be seen with mean square accelerations 0.0076 and 0.026 $\mathrm{m}^2/\mathrm{s}^4$ for rock and alluvium respectively. Fig. 11(b) shows the response spectral densities with different floor-to-column mass ratio, with corresponding mean square as 0.0188, 0.0102 and 0.0076 $\mathrm{m}^2/\mathrm{s}^4$ respectively for $r_{mj} = 0$, 0.1 and 1.

While the aforementioned approach to calculate statistical responses to stochastic ground motion is widely used for seismic design and analysis, it is of interest to note some differences from the conventional one. First, the response calculated in this study is absolute acceleration, not the relative displacement in traditional approach, although they are obtainable from one to the other. More important, the traditional approach assumes that the building is fixed on the ground and subsequently shakes under seismic free-field ground motion, the latter of which is typically characterized by Kanai–Tajimi model with predominant frequency (ω_g) and damping (γ_g) for site amplification. In fact, for a building fixed on the ground, the seismic input at the fixed bottom of a building is the response of soil–structure interaction, not simply the free-field motion. The Fourier spectrum of basement motion in Fig. 8 is a manifest, showing that the motion has no clear predominate frequency. This suggests that either the seismic input in traditional approach needs modified as other type such as band-limited white noise for this case, or the fixed boundary condition is inappropriate. By contrast, this model shows that as long as a motion recording at given location (either at ground or one height) is provided, the statistical response at other location can be obtained.

4. Conclusions

This study proposes a wave-based approach to model and analyze seismic building motion. It first derives the generalized impulse and frequency response functions (GIRF and GFRF) which are fundamentally important in constructing response to the motion input to a system, not the traditional force input. The deterministic and stochastic features of GIRF and GFRF as well as seismic response are also examined in detail, revealing not only well-observed vibration features of building structures, but also some perspective of seismic wave behaviors of structures which traditional vibration-based approach does not show clearly.

While this study focuses on one-dimensional wave propagation with specific shear–beam model for columns/walls and lumped mass for floor, it can be extended to sophisticated modeling such as bending-moment beam model for columns with one extra dimensional wave motion, or another dimension in rocking. While this extension will make the modeling more robust and useful in broad-based applications, the analysis and fundamental features of wave propagation will remain the same as revealed in this study.

Acknowledgments

The authors would like to express their sincere gratitude to S. Al Hilali, A. Abdulla, and M. Al Kurbi from Petroleum Institute in

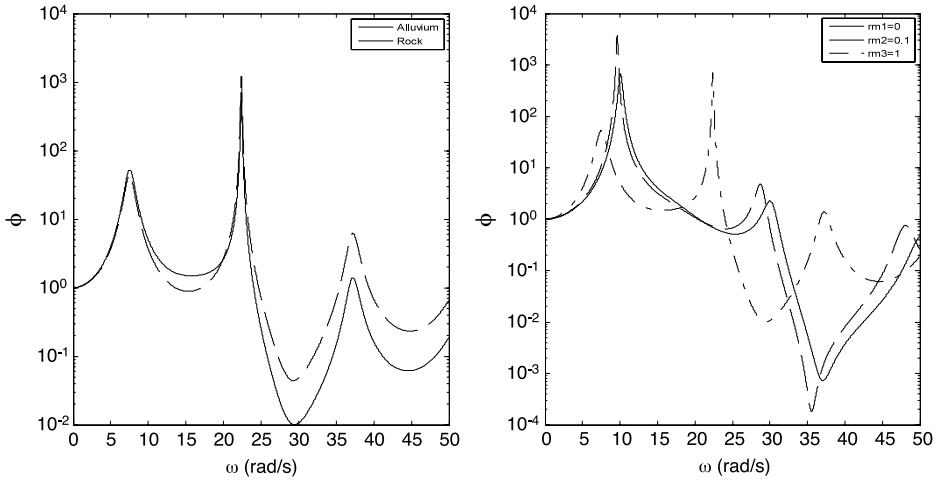

Fig. 11. Spectral density of acceleration at the 8th floor to ground acceleration spectral density with Kanai–Tajimi power spectra ($G_0 = 1$, site predominant frequency ω_g, site damping $\xi_g = 0.34$) with the same building parameters as Fig. 8. (a) (left) $\omega_g = 18.4$ rad/s for alluvium and 27 rad/s for rock, and $r_{mj} = 1$ and (b) (right) $\omega_g = 18.4$ rad/s for alluvium and $r_{mj} = 0$, 0.1 and 1.

United Arab Emirates for providing computational assistance in Section 3.2.

This work was supported by the Colorado School of Mines — Petroleum Institute joint research project under the auspices of Abu Dhabi National Oil Company. The opinions, findings and conclusions expressed herein are those of the authors and do not necessarily reflect the views of the sponsors.

References

[1] Kohler MD, Heaton TH, Bradford SC. Propagating waves in the steel, moment-frame factor building recorded during earthquakes. Bulletin of the Seismological Society of America 2007;97(4):1334–45.
[2] Safak E. Wave-propagation formulation of seismic response of multistory buildings. Journal of Structural Engineering, ASCE 1999;125(4):426–37.
[3] Snieder R, Safak E. Extracting the building response using seismic interferometry: theory and application to the Millikan library in Pasadena, California. Bulletin of the Seismological Society of America 2006;96(2):586–98.
[4] Snieder R, Sheiman J, Calvert R. Equivalence of virtual-source method and wave-field deconvolution in seismic interferometry. Physical Review 2006; E73: 066620 (9 pages).
[5] Todorovska MI, Ivanovic SS, Trifunac MD. Wave propagation in a seven-story reinforced concrete building I: Theoretical models. Soil Dynamics and Earthquake Engineering 2001;21:211–23.
[6] Cai GQ, Lin YK. Localization of wave propagation in disordered periodic structures. AIAA Journal 1991;29(3):450–6.
[7] Lin YK, Wu WF. A closed form earthquake response analysis of multistory building on compliance soil. Journal of Structural Engineering 1984;12(1): 87–110.
[8] Zhang R, Yong Y, Lin YK. Earthquake ground motion modeling. I: Deterministic point source and II: Stochastic line source. Journal of Engineering Mechanics-ASCE 1991;117: 2114–2132 and 2133–2150.
[9] Zhang R. Some observations on modeling of wave motion in a layer-based elastic medium. Journal of Sound and Vibration 2000;229(5): 1193–1212.
[10] Chopra A. Dynamics of structures-theory and applications to earthquake engineering. Prentice-Hall, Inc.; 1995.
[11] Lin YK, Cai GQ. Probabilistic structural dynamics-advanced theory and applications. McGraw-Hill, Inc.; 1995.